JGR Solid Earth

RESEARCH ARTICLE
10.1029/2021JB022614

Further Evidence of High Intensity During the Levantine Iron Age Anomaly in Southwestern Europe: Full Vector Archeomagnetic Dating of an Early Iron Age Dwelling From Western Spain

N. García-Redondo[1], M. Calvo-Rathert[1], Á. Carrancho[2], A. Goguitchaichvili[3], E. Iriarte[4], A. Blanco-González[5], M. J. Dekkers[6], J. Morales-Contreras[3], C. Alario-García[7], and C. Macarro-Alcalde[8]

[1]Departamento de Física, Laboratorio de Paleomagnetismo, Universidad de Burgos, Burgos, Spain, [2]Departamento de Historia, Área de Prehistoria, Geografía y Comunicación, Universidad de Burgos, Burgos, Spain, [3]Servicio Arqueomagnético Nacional y Laboratorio Interinstitucional de Magnetismo Natural, Nacional Autónoma de México, Instituto de Geofísica, Mexico City, México, [4]Departamento de Historia, Laboratorio de Evolución Humana, Geografía y Comunicación, Universidad de Burgos, Burgos, Spain, [5]Departamento de Prehistoria, Historia Antigua y Arqueología, Facultad de Geografía e Historia, Universidad de Salamanca, Salamanca, Spain, [6]Department of Earth Sciences, Paleomagnetic Laboratory Fort Hoofddijk, Utrecht University, Utrecht, the Netherlands, [7]Independent Researcher, Salamanca, Spain, [8]Town Planning Office, Council of Salamanca, Salamanca, Spain

Key Points:

- New high quality full-vector archeomagnetic dating of an Iron Age site in Spain proves to be a more suitable method than ^{14}C for this age
- Intensity-high linked with the Levantine Iron Age Anomaly in Southwestern Europe is corroborated
- A multimethod comparison of Thellier-type and multispecimen paleointensity techniques is performed

Supporting Information:

Supporting Information may be found in the online version of this article.

Correspondence to:

N. García-Redondo,
ngredondo@ubu.es

Citation:

García-Redondo, N., Calvo-Rathert, M., Carrancho, Á., Goguitchaichvili, A., Iriarte, E., Blanco-González, A., et al. (2021). Further evidence of high intensity during the Levantine Iron Age Anomaly in southwestern Europe: Full vector archeomagnetic dating of an Early Iron Age dwelling from Western Spain. *Journal of Geophysical Research: Solid Earth*, *126*, e2021JB022614. https://doi.org/10.1029/2021JB022614

Received 17 JUN 2021
Accepted 31 AUG 2021

Abstract

We report an archeomagnetic study from the Early Iron Age archeological site of Cerro de San Vicente (Salamanca, Spain). The studied materials were sampled from one roundhouse and its central fireplace, a surrounding burnt floor, and slags with a twofold objective. First, to archeomagnetically determine the last use of the central fireplace, because dating with other methods was imprecise. Second, to retrieve information about the Earth's magnetic field in Western Europe from a period when the Levantine Iron Age Anomaly (LIAA) has been occasionally reported. This study includes mineralogical, archeomagnetic directional analyses, and multimethod archeointensity determinations. Paleomagnetic analyses of the central fireplace yield a mean direction: declination $D = 15.1°$, inclination $I = 52.5°$; $k = 477.1$, and $\alpha_{95} = 5.6°$. Archeointensity determinations yield a mean anisotropy-corrected archeointensity of 72.4 ± 2.0 μT (74.7 ± 4.3 μT if a pTRM-check correction is applied) on the central fireplace and 48.2 ± 2.0 μT on slags. A full-vector archeomagnetic dating was performed with the SHA. DIF.4k geomagnetic field model which yielded an age interval of last use of the central fireplace between 644 and 575 BCE (654–575 BCE with the pTRM-check corrected data) at 95% confidence level. This date agrees with the archeological context. Results allows to place the high paleointensity obtained near the maximum observed in Iberia at this age, confirming the existence of this peak related to the LIAA in Western Europe where records of this feature are still scarce.

Plain Language Summary

The direction and the intensity of the Earth's magnetic field (EMF) change with time at a regional scale. Archeomagnetism uses this variation to date burnt archeological materials that have registered the EMF during their last use. We present the archeomagnetic study of a house in Cerro de San Vicente, an Early Iron Age archeological site in Salamanca (Spain). Archeomagnetic dating is especially interesting because other dating techniques like ^{14}C do not yield a precision better than 400 yr in this period. Archeomagnetic data for this period and region are scarce, and our data support the existence of an intensity peak in the EMF for this period and region. The study is focused on the central fireplace of the house, a burnt surrounding floor area, and slags which were found on the floor. The dating obtained for the central fireplace yields an age of 644–575 BCE, determining the last use and the probable abandonment of the house. The dating obtained for slags yields 912–804 BCE, indicating that they are older than the central fireplace. Additionally, we have obtained geoarcheological information related with domestic activities, such as the covering of floors with textile matting items and habitual chores like sweeping.

1. Introduction

Periods, such as the Late Bronze Age (ca. 1,300–900 BCE) and Early Iron Age (ca. 900–400 BCE) in southwestern Europe are very relevant in archeological research because they provide information to reconstruct social and economic changes during a key cultural transition interval (e.g., Gómez-Paccard et al., 2019; Goslar, 2019). The Iberian Peninsula has a rich archeological heritage for this period, but many sites are chronologically still poorly constrained. Combustion structures (e.g., kilns and hearths) and burnt archeological materials (e.g., conflagrated floors, pottery, or slags) are relatively frequent at these sites and represent an excellent opportunity not only to retrieve geomagnetic field information (under the proviso of an independent age control) but also to perform archeomagnetic dating.

Beyond typological seriation, radiocarbon is the most widely used dating method in recent prehistory, but it is not exempt of problems. The occurrence of a plateau in the calibration curve known as the "Hallstatt plateau" (ca. 800–400 BCE) is particularly problematic for this period as it gives rise to a large uncertainty in the date interval not lower than ∼400 yr (Hamilton et al., 2015; Hervé & Lanos, 2017). For this reason, further dating methods are necessary to tackle the Early Iron Age (900–400 BCE) chronology in Western Europe and archeomagnetism is a foremost choice for this period.

Archeomagnetic dating is only applicable in regions with a previously well-established paleo secular variation (PSV) curve or a geomagnetic field model that covers the time span including the target material (e.g., Pavón-Carrasco et al., 2021). Although significant efforts were carried out to compile new directional and intensity data of the Earth's magnetic field (EMF) in the Iberian Peninsula for this period (Molina-Cardín et al., 2018; Osete et al., 2020; Pavón-Carrasco et al., 2021), they are still rather scarce. Regarding the Late Bronze and Early Iron Age, some isolated directional data from the analyses of different combustion structures were reported by Palencia-Ortas et al. (2017) and Molina-Cardín et al. (2018). Recently, 14 new directional data for this time slot in the Iberian Peninsula were provided by Osete et al. (2020). Catanzariti et al. (2008) dated a Late Bronze Age vitrified wall in Portugal and Gómez-Paccard et al. (2019) studied four archeologic hearths from an archeological site in northeast Spain dating their last use to the Early Iron Age. However, as both latter studies applied archeomagnetism for dating purposes, they lack an independent age control, and cannot be included in databases for geomagnetic field modeling purposes.

As far as the archeointensity datasets for this period are concerned, these are even scarcer than paleodirectional data and of variable quality. One of the reasons for the lack of high-quality archeointensity data is the difficulty of carrying out successful and reliable determinations. The scatter of paleointensity results can be high, often because unreliable or erroneous determinations are still considered to represent correct paleointensity results (e.g., Calvo-Rathert et al., 2002). In Thellier-type experiments, certain requirements have to be fulfilled for samples to provide a reliable paleointensity determination: (a) the natural remanent magnetization (NRM) must be a thermoremanent magnetization (TRM); (b) during experiments, no chemical or mineralogical changes should happen (e.g., Kosterov and Prévot, 1998); (c) Thellier laws of reciprocity, independence, and additivity of partial thermoremanence (pTRM) must be obeyed (Thellier & Thellier, 1959). On the other hand, if paleointensity determinations are performed with procedures relying on distinct physical principles, agreement of results will increase their reliability and consistency (e.g., Allington et al., 2021; Calvo-Rathert et al., 2019; de Groot et al., 2013; Monster et al., 2015). Although archeointensity data were obtained from prehistoric materials (mainly pottery) in the Iberian Peninsula (e.g., Burakov et al., 2006; Nachasova & Burakov, 2009), many of them do not fulfill quality criteria or lack necessary information (i.e., anisotropy or cooling rate corrections) to be considered as trustworthy determinations. This is important since the improvement and temporal extension of regional PSV curves or geomagnetic models, should only be carried out with reliable and high-quality data.

Intensity peaks have been observed for the last 4 Kyr in Hawaii (Pressling et al., 2006, 2007) and in Korea circa 3,000 yr ago (Hong et al., 2013). The period around 1,000–500 BCE is characterized by some of the highest intensities observed during Holocene (Genevey et al., 2008). Strong intensity peaks have been observed in China in 1,300 ± 300 BCE (Cai et al., 2017), in Turkey in ∼1,000 BCE (Ertepinar et al., 2012), in Jordan (Ben-Yosef et al., 2009), Israel (Ben-Yosef et al., 2009), or Georgia (Shaar et al., 2017) between the 10th and 8th century BCE, and around 600 BCE in the Canary Islands (Kissel et al., 2015) or Azores (Di Chiara et al., 2014). Specifically, the geomagnetic field in the circum-Mediterranean region shows large

directional and intensity variations during the first millennium BCE (e.g., Osete et al., 2020; Rivero-Montero et al., 2021; Tema et al., 2021). The *Levantine Iron Age geomagnetic Anomaly* (henceforth, LIAA; Shaar et al., 2017) is the most conspicuous field-feature during this time. Although initially the LIAA was considered to show a western limit between 30° and 35°E of longitude (Shaar et al., 2017), later studies suggest that the LIAA features grew in place in the Levant around 1,000 BCE and followed a western migration to arrive in Iberia around 750 BCE (de Groot et al., 2013; Osete et al., 2020; Pavón-Carrasco et al., 2021). In any case, LIAA evidence in southwestern Europe is still tenuous. Hence, the Iberian Peninsula is a good place to verify existing observations.

We report a full-vector archeomagnetic age determination to date an Early Iron Age house in the archeological site of Cerro de San Vicente (CSV; Salamanca, Western Spain). This information is interesting both from a geophysical and archeological point of view. Attempts to date the site by other chronometric techniques (typological comparisons, ^{14}C, and thermoluminescence estimates) provided inaccurate, yielding too large time spans. The possibility of dating the last use (and likely abandonment) of domestic quarters by archeomagnetism offers a good chance to evaluate the potential of the technique for this period, which is archeologically very interesting. Considering the period and region involved (Early Iron Age of South-Western Europe), the prospects of analyzing the full-vector behavior of the EMF studying features like the LIAA, is certainly of high interest from the geomagnetic point of view.

2. Material and Methods

2.1. The Archeological Site and Sampled Dwelling

CSV is located on a flat-topped sandstone plateau (Figure 1a). Archeological excavations at this site (1990–2018) uncovered an Early Iron Age village (ca. 900–400 BCE) with a stone rampart enclosing $\sim 16 \times 10^4$ m^2 (Blanco-González et al., 2017). Its well-preserved mud architecture consisted of informally arranged dwellings with interspersed ancillary buildings and outdoor refuse heaps and winding lanes. Every dwelling was made of sun-dried adobes with a central fireplace and an inner continuous bench. Indoor floors were prepared with multiple layers of clay and crushed sandstone. Interiors surfaces were periodically plastered with clay, from floors to hearths and walls. Excavations revealed frequent superposed buildings. Thus, the walled area yields a thick stratification up to 3–4 m in depth with manifold occupation layers and structures arranged in successive architectural phases.

This paper focuses on the village's summit, where open-area excavations in 2006 and 2017 unearthed 600 m^2 (Figure 1b). This sector produced 4 roundhouses, a central rectangular building, and 13 subsidiary smaller structures. They are all roughly contemporary, from phase III, corresponding to the uppermost layers of the stratigraphic sequence. Dating these layers and structures is a challenge. Dwellings are always devoid of domestic equipment for they were carefully emptied prior to abandonment. The age of phase III can be estimated at 700–600 BCE using chrono-typological criteria. Three radiocarbon essays on long-lived charcoal samples from roundhouses 1, 5, and a nearby midden provide a wide age range calibrated of ca. 820–520 cal BCE.

The sampled dwelling, named House 1, was partly excavated in 2017 (Figure 1c). Its uppermost level had an adobe-paved antechamber to the south, yet no inner mud devices have been identified. At an older phase the house was better-preserved and properly furnished; it featured two benches and a large square fireplace, and a small sounding produced a thick sequence of superimposed floors. This phase also bears proof of an intense fire: soils and surfaces were burnt and covered by a thin ash-rich layer containing slags. After its conflagration, walls were dismantled, and its indoor space was filled with several layers of burnt adobes.

2.2. Archeomagnetic Sampling

In 2017 we took 10 oriented hand-blocks to conduct archeomagnetic directional analysis. Two hand blocks are from the central fireplace and eight from highly burnt parts from the floor surrounding this fireplace. A second sampling was carried out in 2018. The objective was to collect additional hand-blocks where the directional analysis and the magnetic properties had shown positive results. We collected extra samples from the survey-pit north of the central fireplace (two hand-blocks from a thick sequence of overlapping

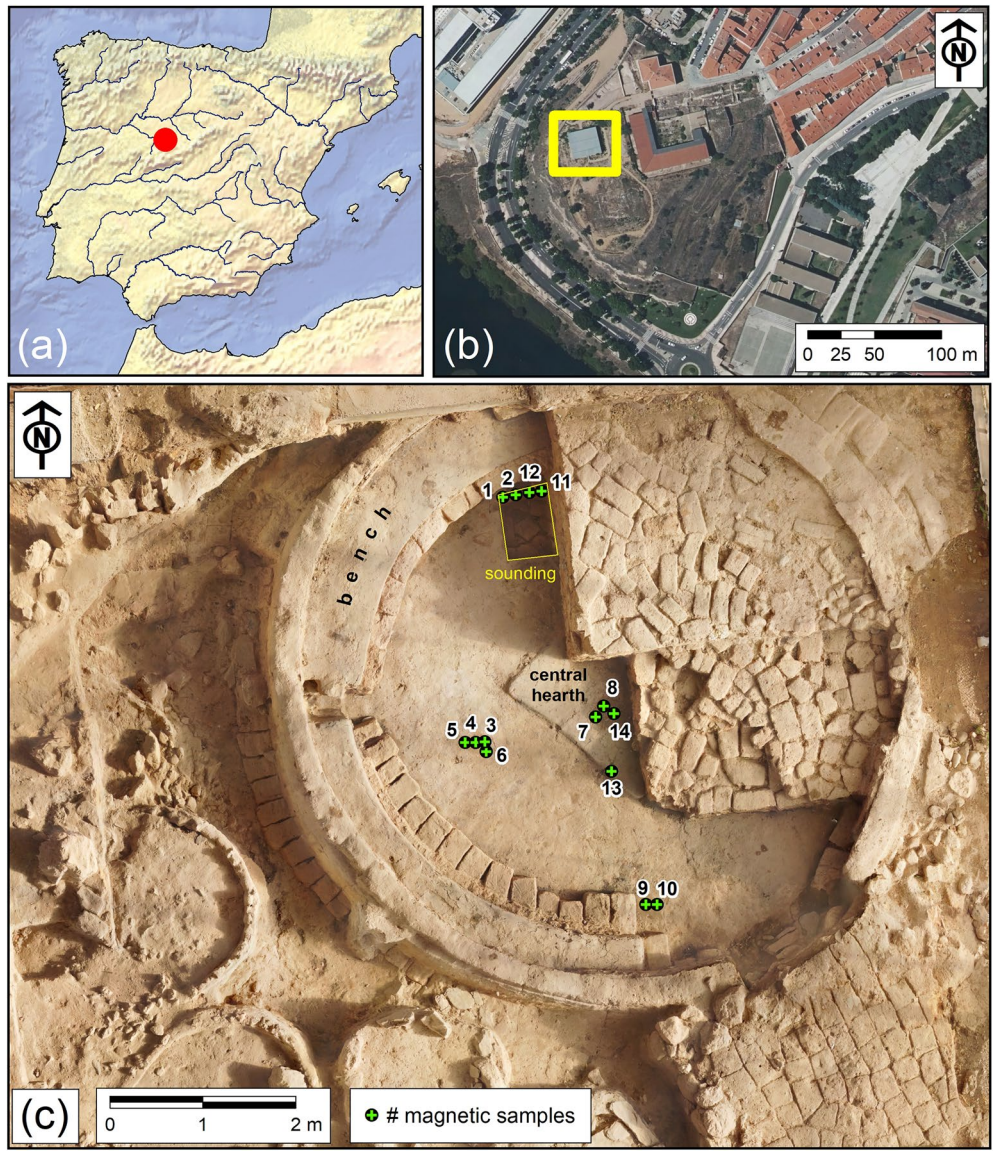

Figure 1. (a) Location of Cerro de San Vicente (Salamanca) in the Iberian Peninsula. (b) Location of the open-area excavation (now roofed) on top of the hill (yellow square). (c) Detail of House 1 with the location of the oriented samples (photogrammetry by Alberto Martín).

occupation floors) and the central fireplace (two hand-blocks). In both samplings, we also collected unoriented material and slags to perform rock-magnetic and archeointensity analyses. These slags were collected from the ashy layer over the soil surrounding the central fireplace (Figure 1c). Hereafter, we will refer to the central fireplace for hand-blocks CSV 7, 8, 13, and14; to the floor for CSV 3, 4, 5, 6, 9, and 10; and to the survey-pit for CSV 1, 2, 11, and 12 (Figure 1c). We collected all hand-blocks following the methodology outlined by García-Redondo et al. (2020).

2.3. Rock-Magnetic Analyses

Rock-magnetic analyses were carried out at the paleomagnetic laboratory of the University of Burgos (Spain). Two powdered samples (~300 mg) from each hand-block and slags were used to identify the main magnetic carriers, their domain state, and their thermal stability, to preselect the most suitable samples for archeointensity experiments. A Variable Field Translation Balance was used to conduct the following

experiments: progressive isothermal remanent magnetization (IRM) acquisition curves up to 1T, hysteresis loops ($\pm 1T$), backfield curves and thermomagnetic magnetization *versus* temperature $M(T)$ curves up to a maximum temperature of 700°C in air. Thermomagnetic curves were performed in a 37 mT field and samples were initially magnetized at room temperature with a 1T field.

Hysteresis parameters were obtained from backfield curves and hysteresis loops. The latter were determined from the hysteresis loops after correction for their dia- or paramagnetic fraction with the *Rock_Mag_Analyzer* software (Leonhardt, 2006). The two-tangent method of Gromme et al. (1969) was used to determine the Curie temperatures (T_c) in the thermomagnetic curves.

2.4. Directional Analyses

Archeomagnetic directional analyses were carried out at the University of Burgos. A 2G SQUID magnetometer (noise level 5×10^{-12} Am^2) was used to measure NRM and samples were subjected either to stepwise thermal (TH) or progressive alternating field demagnetization (AF).

In a pilot study the most appropriate demagnetization sequences were selected. TH demagnetization was done in 11 steps up to maximum temperatures of 550°C–575°C using a TD48-SC (ASC) thermal demagnetizer and AF demagnetization in 11 steps up to maximum fields of 86–100 mT with the demagnetization unit of the 2G magnetometer. After each thermal demagnetization step, magnetic susceptibility was measured with a susceptibility meter KLY-4 (AGICO; noise level $\sim 3 \times 10^{-8}$ SI) to detect possible mineralogical alterations, although this method cannot detect the overall thermal alteration.

The Characteristic Remanent Magnetization (ChRM) direction of all samples was calculated by principal component analysis (Kirschvink, 1980) with the *Remasoft* software (Chadima & Hrouda, 2006). Mean directions were calculated using Fisher statistics (Fisher, 1953).

2.5. Archeointensity Experiments

Archeointensity experiments were carried out at the paleomagnetic laboratory of Burgos University (Spain), at the paleomagnetic laboratory Fort Hoofddijk of Utrecht University (The Netherlands), and at the Archeomagnetic National Service (UNAM) in Morelia (Mexico).

In the Burgos laboratory, the paleointensity experiments were carried out according to the Thellier-type method (Thellier & Thellier, 1959) as modified by Coe (1967) in argon atmosphere using a TD48-SC (ASC) thermal demagnetizer. Remanent magnetization was measured with a 2G SQUID magnetometer. Heating temperature was increased in 11 steps from room temperature to 580°C, applying a laboratory field strength of 40 μT and including four pTRM-checks at 340°C, 420°C, 490°C, and 550°C to check for chemical/mineralogical alterations during the experiments, although satisfying a pTRM check may not completely guarantee the absence of thermal alteration (Wang & Kent, 2021). Temperature reproducibility between the two heating cycles at the same temperature had a precision of ±2°C. We did not measure the cooling rate dependence of the TRM because samples were left cooling down naturally overnight, implying a similar duration as the original cooling time of the samples (Calvo-Rathert et al., 2019).

In the Utrecht paleomagnetic laboratory, paleointensity experiments were performed using the Thellier–IZZI protocol (Yu & Tauxe, 2005). Remanence was measured with a 2G DC-SQUID instrument. To heat the samples, an ASC TD48-SC instrument with in-house developed temperature control was used. The experiment was carried out between room temperature and 590°C in 12 temperature steps with a field strength of 45 μT, applying 6 pTRM-checks after each 4 heating steps (150°C, 220°C, 300°C, 380°C, 460°C, and 520°C). In this experiment sample cooling was fan assisted (30–40 min) and the experiment was performed in air.

Later, we corrected all archeointensity determinations for TRM anisotropy by determining the anisotropy of TRM (ATRM) tensor with the method of Veitch et al. (1984). The ATRM measurements were performed inducing a pTRM (500°C to room temperature with a laboratory field strength of 40 μT) in six sample directions (i.e., $-x$, $+x$, $-z$, $+z$, $-y$, and $+y$) to sister specimens belonging to the same hand block. Hand blocks have a small size, allowing the sampling of highly homogeneous archeological material, which is confirmed also by magnetic experiments like thermomagnetic curves (Figure 2).We followed the same process with

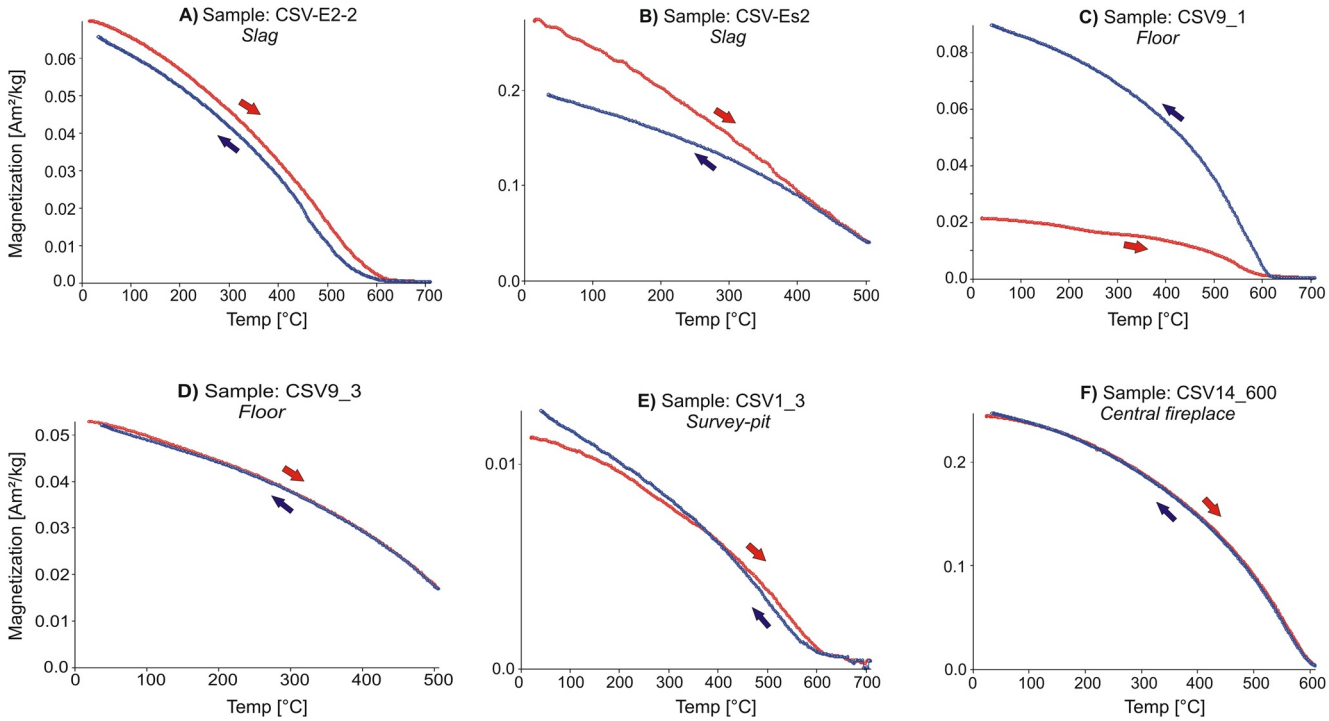

Figure 2. Six representative thermomagnetic curves from slags (a and b), floor (c and d), survey-pit (e), and central fireplace (f). Heating (cooling) cycles are indicated in red (blue) with their respective arrows.

the studied slags, determining the ATRM in five slags collected in the same place as those studied for archeointensity. Before each pTRM acquisition, samples were AF demagnetized at 100 mT, using the remaining magnetization value as a baseline. After the measurement of the pTRM acquired in all six directions, an extra pTRM acquisition step was performed in the same direction as the first step using the same temperature and field to check whether mineralogical changes had occurred during the anisotropy experiment.

Paleointensity data were interpreted using the ThellierTool 4.2 software (Leonhardt et al., 2004). To assess the quality of paleointensity results, we used the ThellierTool criteria thresholds (Leonhardt et al., 2004) as modified by Paterson et al. (2014), differentiating between two quality levels (A and B) of different stringency (Table 1). Arai plots with a clearly concave up shape were discarded, because in such cases remanence is most probably associated to the presence of multidomain (MD) grains (Levi, 1977).

Table 1 shows the paleointensity selection criteria and threshold values. Thellier-type determinations: for quality class A or B. *N*: number of NRM-pTRM points used for archeointensity determination; *f*: fraction of NRM used; *q*: quality factor (Coe et al., 1978); β (β = standard error/absolute slope of the slope of the best fit line); δ(CK): difference between the pTRM check and original TRM value at a given temperature normalized to the TRM (Leonhardt et al., 2000); MAD: mean angular deviation of NRM end-point directions at

Table 1
Thellier-Coe and IZZI Paleointensity Determinations

Thellier-Coe and IZZI paleointensity determinations							
Criteria	*N*	*f*	*q*	β	δ(CK)	MAD (°)	α (°)
Thresholds A	≥5	≥0.5	≥5	≤0.1	≤7	≤6	≤15
Thresholds B	≥5	≥0.35	≥1	≤0.15	≤9	≤15	≤15
Multispecimen paleointensity determinations							
Criteria		R^2		ε_{alt}		Δ*b*/Int	
Thresholds		≥0.9		≤3%		$\lvert\Delta b\rvert \leq 0.15$ and/or within error	

each step obtained from paleointensity experiments; α: angle between the vector average of the data selected for paleointensity determination and the principal component of the data; Multispecimen (MS) determinations: ε_{alt}: Average alteration parameter. R^2: Quality of the linear least-squares fit. Δb/Int: Check of whether the linear fit intersects the ordinate axis through (0–1) within 15% ($\Delta b \leq 0.15$) and/or within error.

In addition to both aforementioned Thellier type experiments, a burnt-floor sample was subjected to the multi-specimen (MS) technique initially proposed by Dekkers and Böhnel (2006). We included the extended protocols for fraction correction (FC) and domain state correction (DSC), both put forward by Fabian and Leonhardt (2010). These experiments were performed in the paleomagnetic laboratory of Morelia, Mexico. A burnt-floor sample was divided into eight specimens which were subsequently immersed into plaster to obtain standard-dimension cylindrical paleomagnetic specimens. The MS method was performed initially at 500°C (based on the Curie temperatures estimated from *M-T* curves) using laboratory fields of 30 and 40 μT. In both cases, the average alteration error (ε_{alt}) was too high (above 5%) to obtain a reliable determination. Consequently, the experiment was halted. Thus, for further measurements, the temperature was reduced to 400°C. Experiments were performed using an ASC Scientific TD48-SC furnace with laboratory fields of 30, 60, and 90 μT. Subsequently, three additional laboratory fields of 45, 70, and 80 μT were applied. For each heating step, the specimens were left heating during 20 min after reaching the selected temperature. Cooling was fan-assisted. The following measurement sequence was applied: (a) measurement of NRM; (b) specimens were oriented in such a way that the NRM directions of each sub specimen lay parallel to the axis of the heating chamber and heated at the corresponding temperature in a laboratory field with this axial direction; (c) specimens were set and heated as in the previous step but inverting the laboratory field direction; (d) specimens were reheated in zero field; (e) step (b) was repeated. After each step (b)–(e), remanence was measured using an AGICO JR6 spinner magnetometer. All calculations were performed employing the VBA software of Monster et al. (2015) and selection criteria and thresholds for a reliable determination are shown on Table 1.

3. Results

3.1. Magnetic Properties

Five samples were selected to study their magnetic properties from the survey-pit, six from the central fireplace, four from the surrounding burnt floor, and three from slags.

All IRM acquisition experiments reach saturation at relatively low fields (Figure S1), indicating that they contain low coercivity ferromagnetic (*s.l.*) minerals. The dominance of low coercivity minerals, probably magnetite and/or maghemite, can be also seen in backfield curves, whose B_{cr} values are between 20 and 40 mT. The saturation IRM (SIRM) is an order of magnitude higher in samples from the slag and the central fireplace, than in the survey-pit and floor samples.

Thermomagnetic curves include a heating cycle (up to 500°C, 600°C, or 700°C) and a cooling cycle. Reversible or nearly reversible curves are found only in slags (Figure 2a), the survey-pit and the central fireplace (Figures 2e and 2f, respectively). Irreversible curves also stem from slags (up to 500°C) and from the floor (up to 700°C; Figures 2b and 2c). Curie temperatures are around 580°C in all samples, suggesting that the main magnetic carrier is Ti-poor titanomagnetite.

On a Day diagram (Day et al., 1977) all samples plot in the pseudo-single domain (PSD) region with a tendency toward the single-domain (SD) region (Figure 3). The use of Day plots for the interpretation of the hysteresis parameters in terms of domain-state can be ambiguous because these parameters are sensitive to several not really specified variables (Roberts et al., 2018). However, samples from this study only contain magnetite, and have a very simple magnetic behavior, reducing the variables affecting the variation in hysteresis parameter ratios. For this reason, in the present study we deem Day plot inferences meaningful as indicative guides.

Analyzing the data from the study with the mixing lines determined by Dunlop (2002) for magnetite, samples from the floor and from the slags seem to have a higher contribution of superparamagnetic (SP) grains than samples from the central fireplace and the survey-pit, which are more clustered in the PSD region.

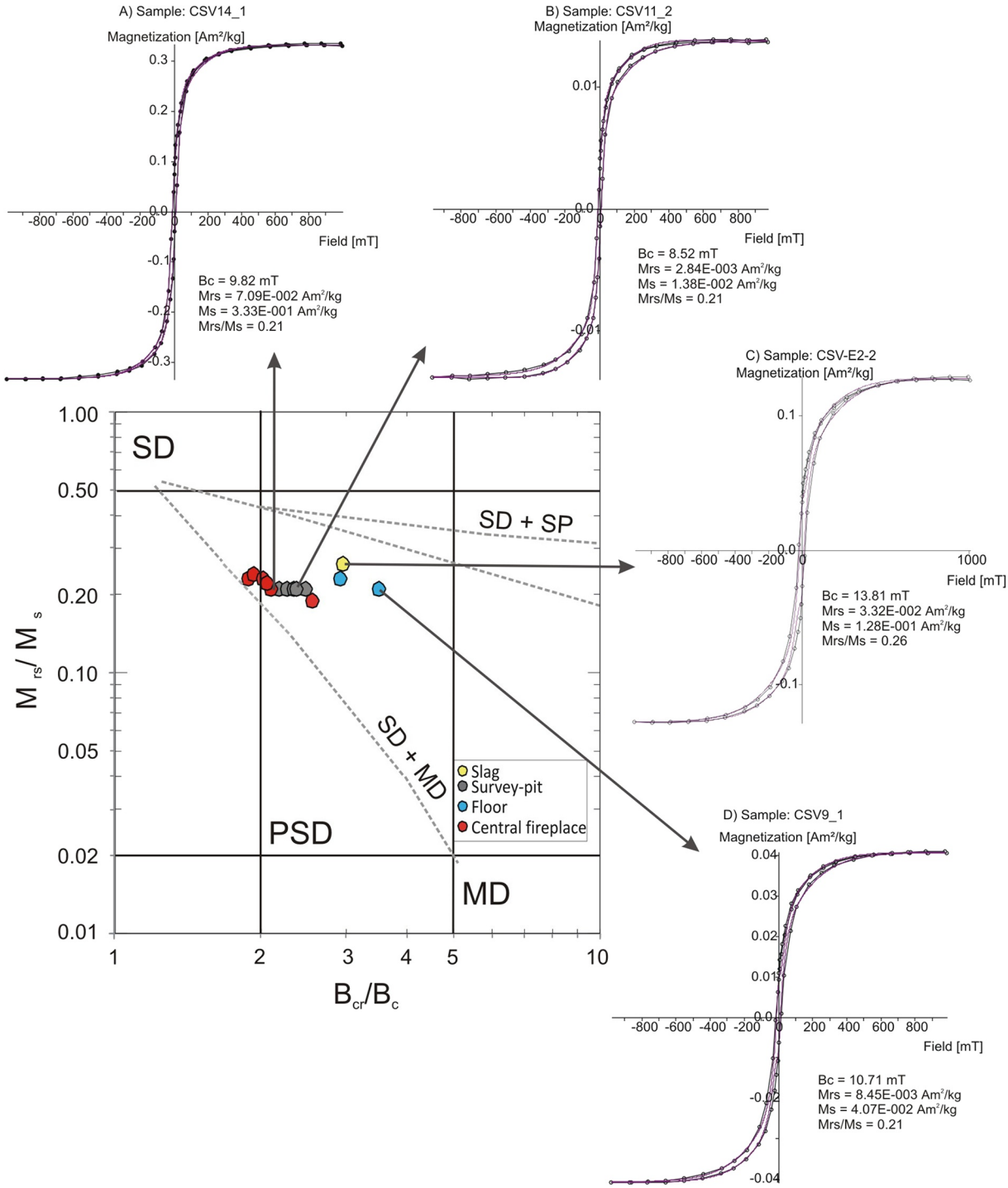

Figure 3. Day et al. (1977) diagram and representative hysteresis loops of four samples from different parts of House 1: central fireplace (a), survey-pit (b), slag (c), and floor (d). Dashed lines in the Day-plot correspond to the mixing trend lines determined by Dunlop (2002) for magnetite. SD (singledomain), PSD (pseudo-singledomain), MD (multidomain), and SP (superparamagnetic).

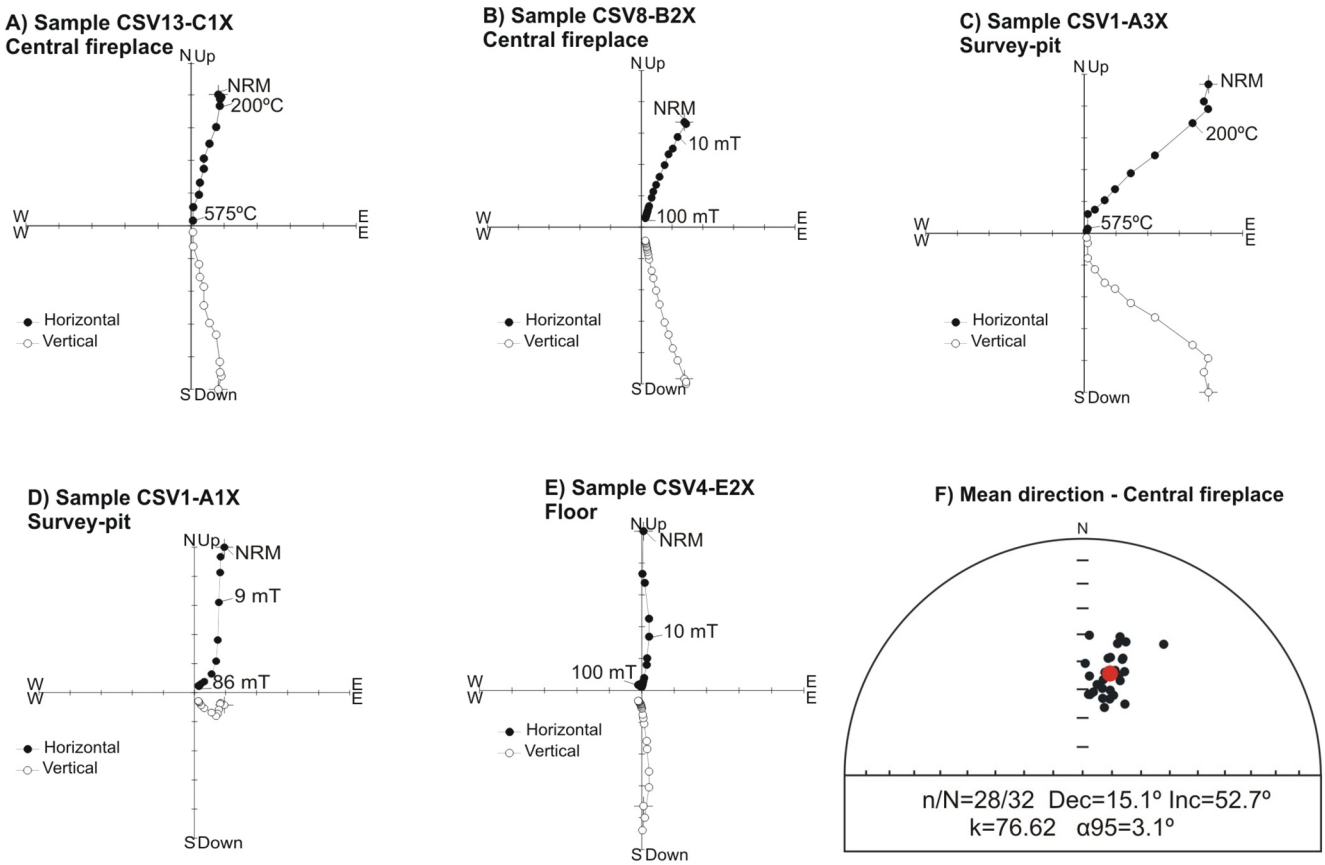

Figure 4. Representative orthogonal NRM demagnetization diagrams showing the behavior during thermal (a) and (c) and alternating field (b, d, and e) demagnetization for the central fireplace samples (a and b), survey-pit samples (c and d) and floor samples (e). Open (Solid) symbols represent the vertical (horizontal) projections of vector endpoints. Sample code and location, main demagnetization steps, and stereogram are shown. (f) Directional results obtained in the central fireplace. [n/N (n = number of specimens considered for the calculation of ChRM/N = number of specimens analyzed); Dec. = declination. Inc. = inclination; α_{95} = radius of 95% confidence cone; k = precision parameter.].

This PSD behavior can be also interpreted as mixture of SD and MD particles with a relatively higher SD contribution. Interestingly, samples from the central fireplace are most SD-like.

3.2. Archeomagnetic Directions

The Königsberger ratio Q_n (Königsberger, 1938; Stacey, 1967), which is the ratio between remanent and induced magnetization, is a useful parameter to characterize burnt archeological materials, allowing the appraisal of the capability of the archeological material to keep a stable remanence. The Q_n ratios (Figure S2) vary between 1.5 and 6.9 in the survey-pit samples; between 1.1 and 12.8 in the floor samples, and between 4.8 and 15.1 in the central fireplace samples. This not only indicates that all studied materials were heated but also that the samples that have best recorded EMF during the last heating and contain more magnetic material are those from the central fireplace.

This fully agrees with the directional results presented next (Figure 4). Samples with good directional results (central fireplace) yield high Q_n ratio values, whereas samples with lower Q_n ratio values (survey-pit and surrounding floor) correspond to directional results with more than one component, lower NRM intensities, and/or very low inclinations.

Depending on the sample origin in the house, significant differences could be recognized in the orthogonal NRM demagnetization diagrams (also named Zijderveld plots). From the central fireplace, three hand-blocks were studied. All specimens have high NRM intensity values (between 2.5×10^{-1} and 1.8×10^{0} Am^2 kg^{-1}) and normal polarity. Susceptibilities vary between 93.8×10^{-5} and 1.16×10^{-3} m^3 kg^{-1}. All show a single

Table 2
Directional Results From the Central Fire

Hand blocks from the central fireplace	*n*/*N*	*D* [°]	*I* [°]	α95	*k*
CSV 8	10/10	15.2	50.7	7.2	46.2
CSV 13	8/11	14.8	50.1	5.2	113.3
CSV 14	10/11	15.2	56.8	3.8	159.6
Central fire (specimen level) $_{(CSV\ 8,\ 13,\ 14)}$	28	15.1	52.7	3.1	76.6
Central fire (hand sample level) $_{(CSV\ 8,\ 13,\ 14)}$	3	15.1	52.5	5.6	477.1

Note. Directional results obtained in the central fireplace from each hand block. Legend as in Figure 4.

component and a weak secondary viscous component easily removable at temperatures of 200°C–250°C with TH demagnetization (Figure 4a) or at 10–20 mT fields with AF demagnetization (Figure 4b). The ChRM directions were isolated between 250°C and 575°C in the TH diagrams (Figure 4a) or between 20 and 100 mT in the AF diagrams (Figure 4b). The NRM values from the survey-pit and the burnt floor are significantly lower (between 5.9×10^{-3} and 3.9×10^{-2} $Am^2\ kg^{-1}$) and more than one component can be distinguished in most Zijderveld plots (Figures 4c–4e). Susceptibilities vary between 47.5×10^{-5} and 8.65×10^{-6} $m^3\ kg^{-1}$.

A total of 28 meaningful results were obtained out of 32 studied specimens, all of them from 3 different hand blocks. The mean direction from House 1 has been calculated considering only the samples from the central fireplace (Figure 4f and Table 2).

Samples from the floor and survey-pit have not been considered because their paleomagnetic behavior shows that these samples have not acquired the TRM observed in the central fireplace. About 4 out of 32 specimens from the central fireplace, 1 from block CSV14, and 3 from CSV13, were not considered for the mean direction (Table 2). One specimen from CSV14 shows an erratic demagnetization behavior due to a mechanical problem with the AF demagnetizer. Two specimens from CSV13 display multicomponent behavior moving away from the origin and the third one has a notably different direction, probably due to an orientation error.

3.3. Archeointensity Results

A total of 27 fragments (14 slags and 13 from the central fireplace) were selected for Thellier-type archeointensity experiments. Whereas in the Thellier-Coe experiment we used argon and let samples cool down in natural conditions, in the Thellier-IZZI experiment we used a cooling fan and the experiment was performed in air. However, the results are the same despite these differences in protocols.

About 13 determinations from the central fireplace were accepted (Table 3). Determinations from hand-block CSV13 were rejected due to the concave shape of the Arai plots. On the other hand, the seven samples from hand-block CSV14 have a very homogenous behavior. Their Arai diagrams, however, display a slight "S" shape with a lower slope in the low-temperature part, a somewhat steeper one in the central part, and a slightly shallower slope at the high temperature end of the diagram (Figure 5a). Coe et al. (2004) observed S-shaped Arai diagrams in a dacite flow, although with a more convex curvature at higher temperatures, that the authors explain as MD behavior. As the samples showed no alteration, paleointensities were determined by Coe et al. (2004) using initial and final points in the Arai diagram. In the present study, all Arai diagrams from specimens of the central fire show only little alteration ($\delta(CK) < 7$, Table 3) and the zero field steps during the paleointensity experiment trend linearly toward the origin, with very low MAD and α values (Table 3), suggesting the absence of remagnetization with unblocking temperatures higher than heating temperatures during the experiment. Thus, we determined paleointensity using all points of the Arai plot. Valet et al. (1996) proposed a correction method to paleointensity determinations based on the difference between the measurement of the original pTRM and the repeated measurement obtained by pTRM-checks. It should be borne in mind that this correction method harbors certain risks, for instance not being able to provide reliable corrected results when alteration is affecting grains with higher blocking temperatures

Table 3
Archeointensity Data for the Studied Specimens

Method	Applied field [μT]	Specimen	Class	T_{min} / T_{max}	N	F	β	dck	q	MAD	α	B_{raw} [μT]	Δb	$B_{An\ corr}$ [μT]
			A		5	0.50	0.10	7	5	6	15			
			B		5	0.35	0.15	9	1	15	15			
Thellier-Coe	40	cs0101 (S)	B	420–580	6	0.50	0.03	5.9	11.0	2.9	0.7	42.5	1.4	44.5
		cs0103 (S)	B	380–580	7	0.92	0.07	7.9	9.0	9.3	3.2	48.5	2.9	50.8
		cs0105 (S)	A	250–580	9	0.89	0.06	6.2	12.6	3.8	1.7	49.3	3	51.6
		cs0106 (S)	A	250–580	9	0.83	0.03	0.4	20.3	4.5	1.7	52.1	1.8	54.6
		cs0107 (S)	B	380–580	7	0.69	0.06	8.9	8.7	3.4	2.4	41.6	2.7	43.5
Thellier-IZZI	45	cs0109 (S)	A	150–550	11	0.92	0.01	1.7	49.6	1.6	0.2	47.4	0.7	49.6
		cs0110 (S)	B	340–550	7	0.69	0.06	5.6	9.3	6.1	8.9	37.3	2.3	39.0
		cs0111 (S)	A	300–590	9	0.79	0.05	2.1	11.7	2.8	1.4	39.1	2.3	40.9
		cs0112 (S)	A	300–550	8	0.70	0.02	2.6	22.3	3.1	1.2	49.5	1.3	51.8
		cs0113 (S)	B	150–590	12	0.91	0.03	6.7	20.5	6.1	3.0	47.5	1.9	49.7
		cs0114 (S)	A	150–550	11	0.86	0.01		55.7	1.8	1.1	51.6	0.7	54.0
		cs0301 (CF)	A	150–590	12	0.85	0.06	5.4	11.3	1.0	0.2	67.4	4.6	72.1
		cs0301 (CF)	A	150–550	11	0.77	0.03		20.7	0.9	0.0	64.1	2.1	68.6
		cs0302 (CF)	A	150–590	12	0.87	0.06	6.6	12.6	1.1	0.7	73.5	4.6	78.6
		cs0302 (CF)	A	150–550	11	0.81	0.02		31.1	1.0	0.9	67.6	1.6	72.3
		cs0303 (CF)	A	150–590	12	0.85	0.07	6.3	10.8	1.5	1.2	77.0	5.5	82.3
		cs0303 (CF)	A	150–550	11	0.78	0.02		26.1	1.4	1.4	69.9	1.9	74.8
		cs0304 (CF)	A	150–590	12	0.86	0.06	4.6	12.8	0.6	0.6	76.7	4.7	82.0
		cs0304 (CF)	A	150–550	11	0.79	0.02		25.6	0.3	0.2	68.8	1.9	73.7
		cs0305 (CF)	A	150–590	12	0.87	0.06	4.5	11.9	0.4	0.2	73.9	4.9	79.0
		cs0305 (CF)	A	150–550	11	0.89	0.04		16.1	0.3	0.3	73.3	3.3	78.5
		cs0306 (CF)	A	150–590	12	0.85	0.07	4.2	9.2	4.4	8.7	67.0	5.2	71.6
		cs0306 (CF)	A	150–550	11	0.58	0.03		15.1	4.2	11.4	74.7	2.5	79.9
Thellier-Coe	40	cs1401 (CF)	A	0–590	11	0.88	0.01	0.65	54.0	6.0	1.0	59.8	0.9	64.0
Multi-specimen				R^2	ε_{alt}				Δb/Int					
				≥0.9	≤3%				$\lvert\Delta b\rvert \le 0.15$ and/or within error					
		CF		0.949	0.949				0.05					68.1
Results										Mean slags		46.0	2.0	48.2
										Mean central fireplace		68.3	2.0	72.4
										Mean central fireplace (Valet et al., 1996)		70.4	4.3	74.7

than the heating temperature (e.g., Tauxe & Yamazaki, 2015). However, we observed that Arai plots from central fireplace specimens lost their S-shape and all points appeared perfectly aligned after application of the correction proposed by Valet et al. (1996). Thus we have additionally determined paleointensities for this sample group applying the Valet-correction for each specimen subjected to this extra determination procedure (Table 3).

A total of 11 determinations (6 class A and 5 class B) were accepted from 14 determinations performed on slags (78.5%) and 7 (class A) from 13 (53.8%) determinations carried out on samples from the central fireplace (Table 3). The fraction factor was rather high, with $f \ge 0.5$ in all cases and $f > 0.75$ in 14 out of 18 cases. Alteration, as shown by alteration parameter (δ(CK)) was generally low. Nine archeointensity

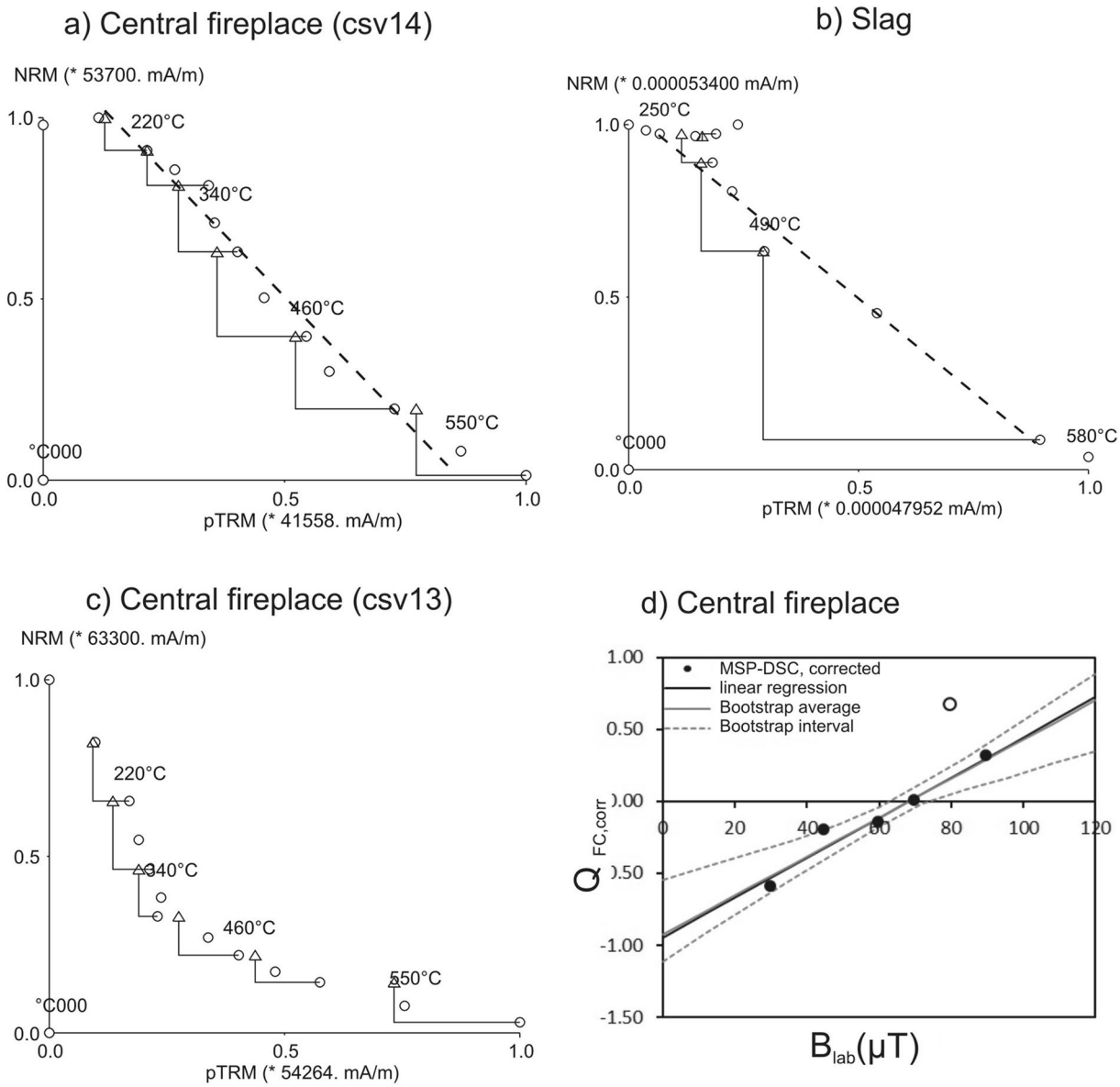

Figure 5. Accepted samples from the Thellier-IZZI (a) and Thellier-Coe (b) experiments. (c) Rejected sample from Thellier-IZZI. (d) Accepted sample from multi-specimen.

determinations (three slags and six from the central fireplace) had to be rejected because of their MD state and their alteration parameter (δ(CK)) exceeding the threshold value (Figure 5c).

The paleointensity mean value obtained for the central fireplace with Thellier-type experiments is 68.3 ± 2.0 and 70.4 ± 4.3 μT if a pTRM-check correction is applied (Valet et al., 1996). After applying the ATRM correction, the mean archeointensity value for the central fireplace with Thellier-type experiments yields $F_{CF,ANIS}$ = 72.4 ± 2.0 μT (74.7 ± 4.3 μT if the Valet et al. (1996); pTRM-check correction is applied). Without ATRM correction, paleointensity for slags yields 46.0 ± 2.0 μT and with correction the mean archeointensity value for slags $F_{S,ANIS}$ = 48.2 ± 2.0 μT.

Furthermore, we have performed a paleointensity determination on the samples from the central fireplace with the MS technique (Dekkers & Böhnel, 2006; Fabian & Leonhardt, 2010), including protocols for FC and DSC (Fabian & Leonhardt, 2010), which is supposed to be independent of the presence of MD grains. If the somewhat anomalous results obtained with the specimen at 80 μT are omitted, all protocols provide reliable

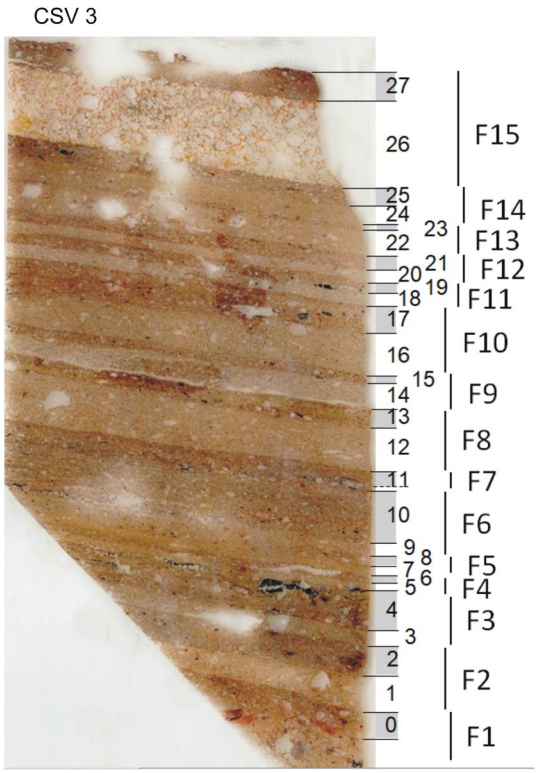

Figure 6. The microstratigraphic sequence of the floor of House 1 indicating the presence of 15 floor phases (F1–F15) composed of prepared floors (white) and activity floors (gray). The thin section size is 13 cm × 7 cm.

determinations (Table S1). We have selected the determination obtained with the fraction and alignment corrected (FCC) protocol (Figure 5d), which yields the best selection criteria values. This experiment confirms the Thellier-type results from the central fireplace discussed above, as an ancient geomagnetic field value of 68.1 μT (N = 5; Min = 62.6 μT; Max = 73.3 μT) is obtained.

Results of the MS experiment were considered as one additional data point to calculate the mean value of the central fireplace. The anisotropy corrected joint result from Thellier-type experiments and MS techniques yields F_{CF} = 72.4 ± 2.0 μT (74.7 ± 4.3 μT with the correction of Valet et al., 1996).

Table 3 shows the archeointensity data for the studied specimens obtained with the Thellier-Coe and Thellier-IZZI protocols [(S) for slags and (CF) for the central fireplace]. Specimen: name of the specimen; $T_{min} - T_{max}$: interval temperature used for the slope calculation; B_{raw}: uncorrected intensity value before anisotropy corrections; $B_{An\ corr}$: intensity value corrected for anisotropy effects. All other column headings as in Table 1.

4. Discussion

4.1. Archeomagnetic Direction and Site-Forming Processes

A mean archeomagnetic direction was obtained from House 1 (Figure 4f and Table 2), considering only samples from the central fireplace. Samples from the other targeted features around the fireplace of House 1 (from the survey-pit and the burnt floor) show a paleomagnetic behavior rather different from the homogenous dynamics observed in samples from the central fireplace itself. Samples from the survey-pit and the floor have much lower NRM values (10^{-2} and 10^{-3} Am^2 kg^{-1}) and more than one component is distinguished in most Zijderveld plots. The directional behavior is erratic in some cases and incoherent between different specimens from the same block. Thermomagnetic curves from the floor and the survey-pit are irreversible and less intense than samples from the central fireplace. However, when samples from the floor are heated up to 700°C, the observed magnetization is as intense as in samples from the central fireplace. Thermomagnetic curves from the floor are still reversible when they are heated up only to 500°C (Figure 2d), but not when heated to 700°C (Figure 2c). This behavior suggests that the central fireplace experienced different archeological thermal processes than the floor. Samples from the central fireplace were heated at high temperature (more than 500°C as shown by thermomagnetic curves) overprinting previous remanences. As no high-temperature record of previous remanences appears in central fireplace specimens, heating could even have reached, at least, 580°C (Curie temperature of magnetite). Samples from the burnt surface around the central fireplace (considering both the survey-pit and the floor) have registered a possible pTRM, which due to the bad quality of the signal cannot be associated with any archeological information. Moreover, as the Q_n ratio values (Figure 2) from the survey-pit and floor are lower than those from the central fireplace, the latter samples have better registered a TRM during the last heating (e.g., García-Redondo et al., 2019, 2020).

To look for an archeological explanation of this pattern, a geoarcheological study of the surface around the central fireplace was performed. Two soil micromorphology blocks were collected from the surface of the survey-pit to carry out thin-section analyses and reconstruct domestic activities. The petrological analysis of the stratigraphic sequence observed in the survey-pit shows 15 refurbishment phases (millimeter thick prepared sand and clay floors; Figure 6) and use of domestic floors, which were flattened by trampling. On these activity floors, sediments were deposited. The nice preservation and characteristics of both types of floors suggest the covering of floors with textile matting items and habitual chores like sweeping, which explains the formation and excellent preservation of these sediments. These sweeping routines are compatible

with the anomalous archeomagnetic behavior described above in samples from the survey-pit and floor. The samples from the floor and survey-pit (F15; Figure 6), correspond to the most recent floor (the uppermost 2 cm; stratigraphic units (SU) SU 26 and SU 27), that is made of a manufactured layer of quartz sand and a clay matrix (SU 26) on which a layer of compacted clay (SU27) was placed. Figure 6 shows that in prepared soils (SU27) all grains have the long axis parallel to the surface due to compaction during preparation and trampling. In addition, as mentioned above, floors are less thermochemically altered than the central fireplace. They did not undergo heating temperatures as high as those from the central fireplace, in good agreement with the magnetic property results.

Therefore, the high heating temperatures (>600°C–700°C) only affected the central fireplace, allowing registering correctly the EMF during its last heating. For this reason, the mean direction at specimen level was calculated only with samples from this feature (Table 2).

4.2. Archeointensity Results

Archeointensity mean values were determined for the slags and for the central fireplace. In the latter case, an additional mean value was calculated after applying Valet's et al. (1996) correction method. The mean value obtained from the central fireplace includes Thellier and MS methods, increasing the robustness of the results. Successful determinations were obtained in 11 of 14 slags and in 9 of 17 specimens from the central fireplace. This relatively low success rate is common in prehistoric hearths due to the poor preservation of combustion structures, and the mineralogy and burial conditions.

Results obtained from slags and the central fireplace samples are diverse, indicating that the remanence of both types of samples is not contemporaneous. Given that archeointensity values obtained in both areas differ, the last heating that affected the central fireplace was not the one that altered the slags. Otherwise, the mean archeointensity values would have been comparable or even the same and that is not the case. Slags (very small debris) lie over the last soil of House 1 around the central fireplace, yet they seem erratic residues taken from elsewhere, most likely from the nearby middens where slags are frequent. This is indeed demonstrated by the archeointensity dating results on slags discussed below (Section 4.3). The suitability of slags for archeointensity research has been reported elsewhere (e.g., Ben-Yosef et al., 2009; Shaar et al., 2015). Considering the relative abundance of this type of material in later prehistoric sites, its study should attract even more attention.

4.3. Archeomagnetic Dating

For archeointensity dating we used the SHA.DIF.4k geomagnetic field model (Pavón-Carrasco et al., 2021) that describes the variations of the EMF for the last 4,000 yr using exclusively archeomagnetic and volcanic data. To carry out the dating, the Matlab archeomagnetic dating tool (Pavón-Carrasco et al., 2011) was used. When multiple solutions are obtained, the choice of the most probable age interval will depend on the archeological context. The archeomagnetic dating of the central fireplace at specimen level was carried out considering the full magnetic field vector. For slags only the intensity could be considered.

Of the different age ranges obtained for the central fireplace, the most plausible with the archeological context are 644 and 575 BCE or between 654 and 575 BCE both at 95% probability (Figures 7a and 7b). The second interval is based on pTRM-corrected intensity data (Valet et al., 1996) and both results are practically the same. Considering the archeological context, the last use of the central fireplace most probably was between the seventh and sixth centuries BCE. Adding the archeointensity value does not significantly constrains the age of last use because considering only the direction the interval obtained is between 662 and 576 BCE (not shown here). However, archeointensity values are of great value to identify specific geomagnetic features as discussed below (Section 4.4). It is worth recalling that from ca. 800 to 400 BCE the radiocarbon calibrated curve does not distinguish ranges lower than ~400 yr because of the "Hallstatt plateau" (Hervé & Lanos, 2017). Therefore, this archeomagnetic age determination is of great value because of the other absolute dating methods applied to House 1 (namely ^{14}C and OSL techniques) failed determining the age of this occupation with similar precision.

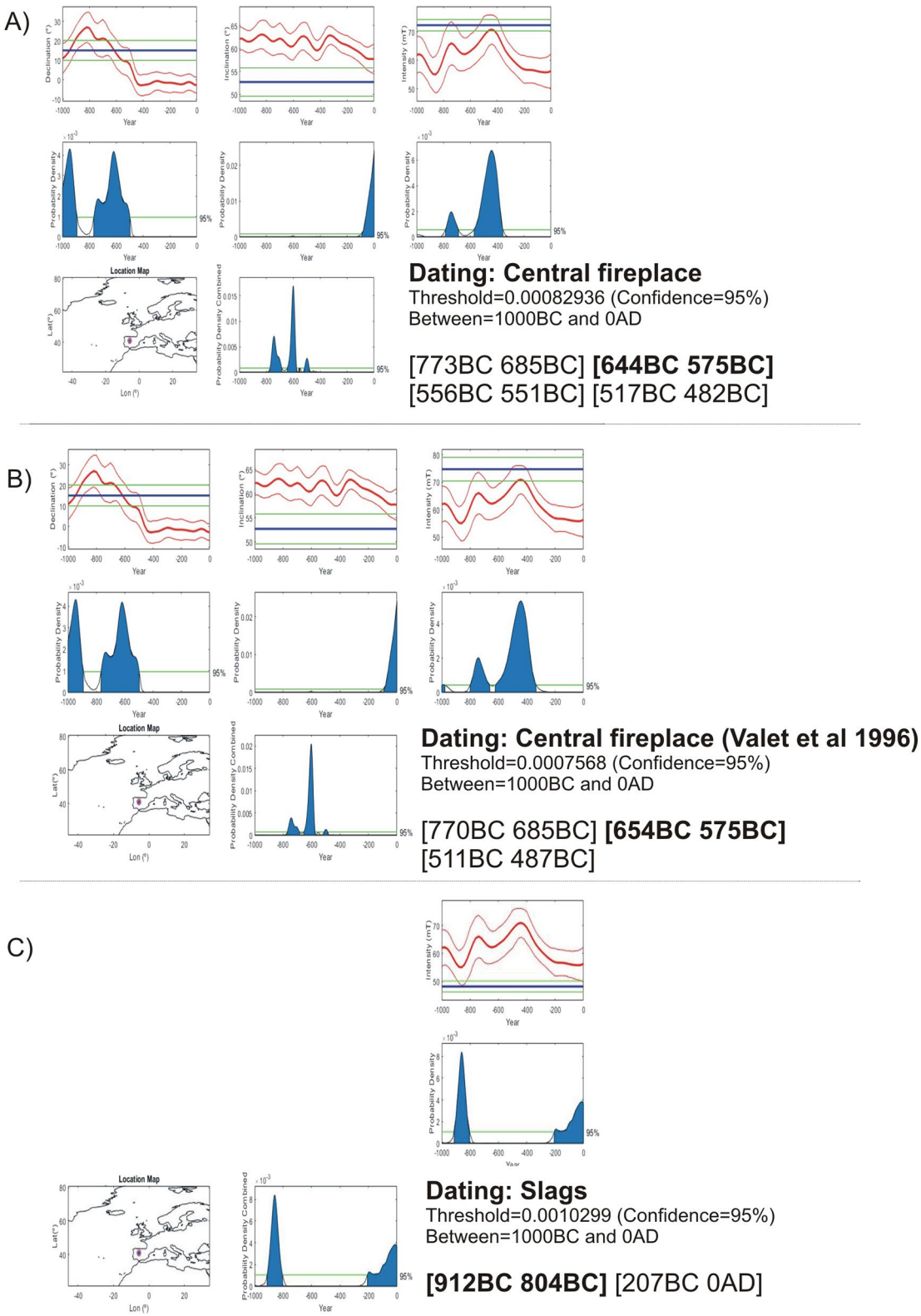

Figure 7. Archeomagnetic dating results obtained for the central fireplace in the *House 1* (a), for the central fireplace based on Valet et al. (1996) (b) and slags (c). Age probability density functions obtained with the MATLAB tool of Pavón-Carrasco et al. (2011) comparing the SHA.DIF.4k model with the declination (left), inclination (middle), and intensity values (right) at site coordinates. Results are expressed at 95% probability.

Slags were dated using only the intensity parameter (Figure 7c). Two different intervals are possible, but no one is coherent with the archeological context. The determinations obtained are technically correct and based on different experimental protocols (Table 3), so we deem the results robust. If we accept the interval 912 and 804 BCE as the most plausible due to its chronological closeness to the expected archeological age (ca. seventh century BCE—also confirmed by archeomagnetism), it would be necessary to explain why these slags found around the central fireplace are between 1 and 4 centuries older than the fireplace. We emphasize that the intensity recorded in the central fireplace and in the slags is neatly different. Interestingly, slag formation requires very high temperatures (e.g., Montero Ruiz & Ruiz Taboada, 1996), which was not the case of the sampled floor as proved by the results of rock-magnetic analyses. Therefore, the slags over that surface can only be accounted for envisaging their intentional deposition there, long time after their ignition, a burning event that clearly predated the last ignition of the central fireplace. For the moment, we cannot determine more precisely these formation dynamics. In any case, slags clearly predate the central fireplace.

4.4. The Behavior of the Earth's Magnetic Field

Iberian directional data for the period between ca. 1,250 and 500 yr BCE (Late Bronze-Early Iron Ages) include 18 determinations (Molina-Cardín et al., 2018; Osete et al., 2020; Palencia-Ortas et al., 2017). In contrast, the archeointensity data between 1,400 BCE and 0 AD are more numerous. However, most of them do not fulfill quality criteria because they do not have ATRM or cooling rate corrections or are only based on one single specimen (e.g., Burakov et al., 2006; Nachasova & Burakov, 2009; Nachasova et al., 2007). Fortunately, now more new reliable archeointensity data for the first millennium BCE for Iberia (Molina-Cardín et al., 2018; Osete et al., 2016, 2020) are available. But to better constrain the EMF evolution for the Late Bronze-Early Iron Ages in Western Europe more data are needed.

The lack of an independent age control at the site (beyond the relative age control provided by archeological constraints), prevents us to use the full-vector archeomagnetic results obtained as input data for the improvement of the Iberian PSVC. Nevertheless, the high-intensity values obtained for the central fireplace (ca. 70–80 μT) strongly suggest a record of a special geomagnetic feature characterized by a markedly higher intensity. Taking into account the archeomagnetic dating results for the central fireplace (ca. seventh century BCE), in good agreement with archeological observations, our high archeointensities confirm the existence of a peak in Southwestern Europe related to the LIAA (Molina-Cardin et al., 2018; Osete et al., 2020). This result advances our understanding of the EMF during events like LIAA. Although there are still few data available, the presence of the LIAA in SW Europe seems to be related to a non-dipolar magnetic anomaly at the core mantle boundary (Osete et al., 2020). The maximum around 500 BCE was simultaneous from Western Europe to Turkey, and probably in Central Asia (Rivero-Montero et al., 2021).

The most recent model study of LIAA's evolution for the European continent and adjacent areas indicate that it is defined by two short-decadal intensity variations with high values up to 100 μT around 950 and 700 BCE (Pavón-Carrasco et al., 2021). With regard to the Iberian Peninsula, the recent high-quality PSVC for the last three millennia (Molina-Cardín et al., 2018) shows high intensities (∼80 μT) around 600 BCE, which are related to eastern declinations (around 20°), also observed in the present study. This evolution shows fast secular variation rates up to 16 μT per century (Osete et al., 2020). In addition, the data compiled from the Middle East to Iberia suggest that the LIAA follows a western migration pattern from the Levant region (Osete et al., 2020; Rivero-Montero et al., 2021; Shaar et al., 2017; Tema et al., 2021). However, Rivero-Montero et al. (2021) suggest that the LIAA extends from the Levantine region to the east and to the west with different rates. Our high intensity values are close to this intensity maximum (Figure 7), providing new and archeologically well age constrained evidence of the LIAA in south-western Europe. This contributes with more new reliable archeointensity data for the first millennium BCE for Iberia to improve the knowledge of the LIAA.

5. Conclusions

An archeomagnetic and archeointensity study was carried out in House 1 from the Early Iron Age archeological site of CSV (Salamanca, Spain). The study of this dwelling entailed sampling a central fireplace and a surrounding burnt surface, which included a floor, slags, and a sequence of soils below the floor exposed in a survey-pit. This study yields the following conclusions:

Archeomagnetic results were obtained from the central fireplace. These specimens show intense magnetizations and directions with normal polarity. The mean direction obtained is: declination $D = 15.1°$, inclination $I = 52.7°$; $k = 76.6$; $\alpha_{95} = 3.1°$ at specimen level or $D = 15.1°$, $I = 52.5°$; $k = 477.1$; $\alpha_{95} = 5.6°$ at sample level.

The floor and the survey-pit samples show different magnetic properties and paleomagnetic characteristics indicating that these parts of the house have not been heated to the same high temperatures experienced by the central fireplace. Before performing this study, the archeological presumption was that the central fireplace and the surrounding burnt surface had experimented the same heating process.

Successful archeointensity determinations were obtained through three methods: Thellier-Coe, Thellier-IZ-ZI, and MS on 20 specimens. About 9 successful absolute archeointensity determinations were obtained from specimens from the central fireplace and 11 from slags. After anisotropy correction, the mean archeointensity value for the central fireplace with the three methods is 72.4 ± 2.0 or 74.7 ± 4.3 μT (the latter applying the correction proposed by Valet et al., 1996) and 48.2 ± 2.0 μT for slags with Thellier-Coe and Thellier-IZZI.

The comparison of the mean directional and intensity values from the central fireplace with the SHA. DIF.4k geomagnetic model resulted in two different age intervals of last use at the 95% confidence level: 644–575 BCE (654–575 BCE with the Valet et al., 1996 correction) which agrees well with the archeological context, indicating with high probability the date of the last use of the central fireplace. This result provides a high-precision constraint on the archeological dating estimates. In addition, it is especially valuable because only very few archeomagnetic dates exist in prehistoric sites based on full vector data.

So far, the slags were considered contemporaneous to the central fireplace. However, the comparison of the mean archeointensity value with the SHA.DIF.4k geomagnetic model allows to conclude that they are between 1 and 4 centuries older. Whether they were intentionally deposited over the sampled burnt floor or they ended up there by an unnoticed process is still unclear and requires further investigation.

This study demonstrates how archeomagnetism markedly improves age dating with respect to radiocarbon dating that has only a poor resolution in the age range of 800–400 BCE.

This study also demonstrates and confirms the presence of the LIAA in Iberia, in Western Europe where records of this anomalous feature are still scarce.

Acknowledgments
N.G.R. acknowledges the financial support given by the Junta de Castilla y León and the European Research and Development Fund (ERDF). Financial support for this work was obtained from Junta de Castilla y León (project BU235P18) and the European Regional Development Fund (ERDF) and the PID2019-105796GB-I00 of the Agencia Estatal de Investigación (AEI/10.13039/501100011033). Special thanks are also due to the "Fort Hoofddijk" paleomagnetic group in Utrecht University for their support and help during a short internship carried out by one of us (N.G.R). A.B.G. acknowledges the Council of Salamanca and the research project PID2019-104349GA-I00 funded by the Spanish Ministry of Science and Innovation. Huapei Wang and an anonymous reviewer as well as editor Isabelle Manighetti are acknowledged for their constructive and helpful review and comments, which helped to improve the manuscript.

Data Availability Statement

Data sets for this research are available under the following reference: García-Redondo et al. (2021), https://doi.org/10.5281/zenodo.4964279.

References

Allington, M. L., Batt, C. M., Hill, M. J., Nilsson, A., Biggin, A. J., Card, N., & Card, N. (2021). Obtaining archaeointensity data from British Neolithic pottery: A feasibility study. *Journal of Archaeological Science: Reports*, *37*, 102895. https://doi.org/10.1016/j.jasrep.2021.102895

Ben-Yosef, E., Tauxe, L., Levy, T. E., Shaar, R., Ron, H., & Najjar, M. (2009). Geomagnetic intensity spike recorded in high resolution slag deposit in Southern Jordan. *Earth and Planetary Science Letters*, *287*, 529–539. https://doi.org/10.1016/j.epsl.2009.09.001

Blanco-González, A., Alario García, C., & Macarro Alcalde, C. (2017). The earliest villages in Iron Age Iberia (800–400 BC): A view from Cerro de San Vicente (Salamanca, Spain). *Documenta Praehistorica*, *44*, 386–401. https://doi.org/10.4312/dp.44.24

Burakov, K. S., Nachasova, I. E., & Mata, C. (2006). Geomagnetic field intensity in the first millennium BC from data on ceramics of the Los Villares archaeological monu-ment (Spain). *Izvestiya, Physics of the Solid Earth*, *11*, 942–950. https://doi.org/10.1134/s1069351306110073

Cai, S., Jin, G., Tauxe, L., Deng, C., Qin, H., Pan, Y., & Zhu, R. (2017). Archaeointensity results spanning the past 6 kiloyears from eastern China and implications for extreme behaviors of the geomagnetic field. *Proceedings of the National Academy of Sciences of the United States of America*, *114*(1), 39–44. https://doi.org/10.1073/pnas.1616976114

Calvo-Rathert, M., Morales, J., Carrancho, A., Camps, P., Goguitchaichvili, A., & Hill, M. J. (2019). Reproducibility of archaeointensity determinations with a multimethod approach on archaeological material reproductions. *Geophysical Journal International*, *218*(3), 1719–1738. https://doi.org/10.1093/gji/ggz246

Calvo-Rathert, M., Prevot, M., Perrin, M., & Riisager, J. (2002). Investigating the reasons for the failure of palaeointensity experiments: A study on historical lava flows from Mt. Etna. (Italy). *Geophysical Journal International*, *149*, 44–63. https://doi.org/10.1046/j.1365-246X.2002.01619.x

Catanzariti, G., McIntosh, G., Soares, A. M. M., Díaz-Martínez, E., Kresten, P., & Luisa, O. M. (2008). Archaeomagnetic dating of a vitrified wall at the Late Bronze Age settlement of Misericordia (Serpa, Portugal). *Journal of Archaeological Science*, *35*(5), 1399–1407. https://doi.org/10.1016/j.jas.2007.10.004

Chadima, M., & Hrouda, F. (2006). Remasoft 3.0 a user-friendly palaeomagnetic databrowser and analyzer. *Travaux Géophysiques*, *XXVII*, 20–21.

Coe, R. S. (1967). Paleointensities of the earth's magnetic field determined from tertiary and quaternary rocks. *Journal of Geophysical Research*, *72*(12), 3247–3262. https://doi.org/10.1029/JZ072i012p03247

Coe, R. S., Grommé, S., & Mankinen, E. A. (1978). Geomagnetic paleointensities from radiocarbon- dated lava flows on Hawaii and the question of the Pacific non-dipole low. *Journal of Geophysical Research*, *83*(B4), 1740–1756. https://doi.org/10.1029/JB083iB04p01740

Coe, R. S., Riisager, J., Plenier, G., Leonhardt, R., & Krása, D. (2004). Multidomain behavior during Thellier paleointensity experiments: Results from the 1915 Mt. Lassen flow. *Physics of the Earth and Planetary Interiors*, *147*, 141–153. https://doi.org/10.1016/j.pepi.2004.01.010

Day, R., fuller, M., & Schmidt, V. A. (1977). Hysteresis properties titanomagnetites: Grain size and compositional dependence. *Physics of the Earth and Planetary Interiors*, *13*, 260–267. https://doi.org/10.1016/0031-9201(77)90108-x

de Groot, L. V., Biggin, A. J., Dekkers, M. J., Langereis, C. G., & Herrero-Bervera, E. (2013). Rapid regional perturbations to the recent global geomagnetic decay revealed by a new Hawaiian record. *Nature Communications*, *4*, 1–7. https://doi.org/10.1038/ncomms3727

Dekkers, M. J., & Böhnel, H. N. (2006). Reliable absolute palaeointensities independent of magnetic domain state. *Earth and Planetary Science Letters*, *248*, 508–517. https://doi.org/10.1016/j.epsl.2006.05.040

Di Chiara, A., Tauxe, L., & Speranza, F. (2014). Paleointensity determination from São Miguel (Azores Archipelago) over the last 3 ka. *Physics of the Earth and Planetary Interiors*, *234*, 1–13. https://doi.org/10.1016/j.pepi.2014.06.008

Dunlop, D. J. (2002). Theory and application of the Day plot (Mrs/Ms versus Hcr/Hc) 2. Application to data for rocks, sediments, and soils. *Journal of Geophysical Research: Solid Earth*, *107*(B3), 2057. https://doi.org/10.1029/2001JB000487

Ertepinar, P., Langereis, C. G., Biggin, A. J., Frangipane, M., Matney, T., Ökse, T., & Engin, A. (2012). Archaeomagnetic study of five mounds from Upper Mesopotamia between 2500 and 700 BCE: Further evidence for an extremely strong geomagnetic field ca. 3000 years ago. *Earth and Planetary Science Letters*, *357*–358, 84–98. https://doi.org/10.1016/j.epsl.2012.08.039

Fabian, K., & Leonhardt, R. (2010). Multiple-specimen absolute paleointensity determination: An optimal protocol including pTRM normalization, domain-state correction, and alteration test. *Earth and Planetary Science Letters*, *297*, 84–94. https://doi.org/10.1016/j.epsl.2010.06.006

Fisher, R. (1953). Dispersion on a sphere. *Proceedings of the Royal Society A: Mathematical, Physical and Engineering Sciences*, *217*, 295–305. https://doi.org/10.1098/rspa.1953.0064

García-Redondo, N., Carrancho, Á., Goguitchaichvili, A., Morales, J., Calvo-Rathert, M., & Palomino, A. (2020). New constraints on the medieval repopulation process in the northern Iberian plateau from the full vector archaeomagnetic dating of two hearths at La Pudia site (Caleruega, Burgos, Spain). *Archaeological and Anthropological Sciences*, *12*, 91. https://doi.org/10.1007/s12520-020-01041-1

García-Redondo, N., Carrancho, Á., Goguitchaichvili, A., Morales, J., & Palomino, A. (2019). Comprehensive magnetic surveys of kilns for bell and tile fabrication in Castile (Spain). *Journal of Archaeological Science: Reports*, *23*, 426–436. https://doi.org/10.1016/j.jasrep.2018.11.003

García-Redondo, N., Goguitchaichvili, A., & Morales, J. (2021). *Rock-magnetic, paleomagnetic and multimethod paleointensity in Cerro de San Vicente archaeological site (Salamanca, Spain). [Data set]*. Zenodo. Retrieved from https://doi.org/10.5281/zenodo.4964279

Genevey, A., Gallet, Y., Constable, C. G., Korte, M., & Hulot, G. (2008). ArcheoInt: An upgraded compilation of geomagnetic fieldintensity data for the past ten millennia and its application to the recovery of the past dipole moment. *Geochemistry, Geophysics, Geosystems*, *9*(4). https://doi.org/10.1029/2007GC001881

Gómez-Paccard, M., Rivero-Montero, M., Chauvin, A., García i Rubert, D., & Palencia-Ortas, A. (2019). Revisiting the chronology of the Early Iron Age in the north-eastern Iberian Peninsula. *Archaeological and Anthropological Sciences*, *11*, 4755–4767. https://doi.org/10.1007/s12520-019-00812-9

Goslar, T. (2019). The chronology and periodization of the Bronze and the early Iron Age burial ground in Domasław, Wrocław district, based on radiocarbon dating. *Przegląd Archeologiczny*, *67*, 31–48. https://doi.org/10.23858/PA67.2067.2019.002

Gromme, C. S., Wright, T. L., & Peck, D. L. (1969). Magnetic properties and oxidation of iron-titanium oxide minerals in alae and Makaopuhi Lavalakes, Hawaii. *Journal of Geophysics Research*. *74*, 5277.

Hamilton, W. D., Haselgrove, C., Gosden, C. (2015). The impact of Bayesian chronologies on the British Iron Age. *World Archaeology*, *47*(4), 642–660. https://doi.org/10.1080/00438243.2015.1053976

Hervé, G., & Lanos, P. (2017). Improvements in archaeomagnetic dating in western Europe from the late bronze to the late iron ages: An alternative to the problem of the Hallstattian radiocarbon plateau. *Archaeometry*, *60*(4), 870–883. https://doi.org/10.1111/arcm.12344

Hong, H., Yu, Y., Lee, C. H., Kim, R. H., Park, J., Jingyu, D., et al. (2013). Globally strong geomagnetic field intensity circa 3000 years ago. *Earth and Planetary Science Letters*, *383*, 142–152. https://doi.org/10.1016/j.epsl.2013.09.043

Kirschvink, J. L. (1980). The least-square line and plane and the analysis of paleomagnetic data. *Geophysical Journal International*, *62*, 699–718. https://doi.org/10.1111/j.1365-246x.1980.tb02601.x

Kissel, C., Laj, C., Rodríguez-Gonzalez, A., Perez-Torrado, F., Carracedo, J. C., & Wandres, C. (2015). Holocene geomagnetic field intensity variations: Contribution from the low latitude Canary Islands site. *Earth and Planetary Science Letters*, *430*, 178–190. https://doi.org/10.1016/j.epsl.2015.08.005

Königsberger, J. G. (1938). Natural residual magnetism of eruptive rocks. *Terrestrial Magnetism and Atmospheric Electricity*, *43*, 299–320.

Kosterov, A., & Prévot, M. (1998). Possible mechanism causing failure of Thellier paleointensity experiments in some basalts. *Geophysics Journal of International*, *134*, 554–572.

Leonhardt, R. (2006). Analyzing rock magnetic measurements: The RockMagAnalyzer 1.0 software. *Computers & Geosciences*, *32*, 1420–1431. https://doi.org/10.1016/j.cageo.2006.01.006

Leonhardt, R., Heunemann, C., & Krasa, D. (2004). Analyzing absolute paleointensity determinations: Acceptance criteria and the software ThellierTool 4.0. *Geochemistry, Geophysics, Geosystems*, *5*(12). https://doi.org/10.1029/2004GC000807

Leonhardt, R., Hufenbecher, F., Heider, F., & Soffel, H. (2000). High absolute paleointensity during a mid Miocene excursion of the Earth's magnetic field. *Earth and Planetary Science Letters*, *184*, 141–154. https://doi.org/10.1016/s0012-821x(00)00311-3

Levi, S. (1977). The effect of magnetite particle size on paleointensity determinations of the geomagnetic field. *Physics of the Earth and Planetary Interiors*, *13*(4), 245–259. https://doi.org/10.1016/0031-9201(77)90107-8

Molina-Cardín, A., Campuzano, S. A., Osete, M. L., Rivero-Montero, M., Pavón-Carrasco, F. J., Palencia-Ortas, A., et al. (2018). Updated Iberian archeomagnetic catalogue: New full vector paleosecular variation curve for the last three millennia. *Geochemistry, Geophysics, Geosystems*, *19*, 3637–3656. https://doi.org/10.1029/2018gc007781

Monster, M. W. L., de Groot, L. V., Biggin, A. J., & Dekkers, J. M. (2015). The performance of various palaeointensity techniques as a function of rock magnetic behavior—A case study for La Palma. *Physics of the Earth and Planetary Interiors*, *242*, 36–49. https://doi.org/10.1016/j.pepi.2015.03.004

Montero Ruiz, I., & Ruiz Taboada, A. (1996). Enterramiento colectivo y metalurgia en el yacimiento Neolítico de Cerro Virtud (Cuevas de Almanzora, Almería). *Trabajos de Prehistoria*, *53*(2), 55–75. https://doi.org/10.3989/tp.1996.v53.i2.392

Nachasova, I. E., & Burakov, K. S. (2009). Variation of the intensity of the Earth's magnetic field in Portugal in the 1st Millennium BC. *Izvestiya, Physics of the Solid Earth*, *45*(7), 595–603. https://doi.org/10.1134/s1069351309070040

Nachasova, I. E., Burakov, K. S., Molina, F., & Cámara, J. (2007). Archaeomagnetic study of ceramics from the Neolithic Los Castillejos multilayer monument (Montefrio, Spain). *Physics Solid Earth*, *43*, 170–176. https://doi.org/10.1134/S1069351307020073

Osete, M. L., Chauvin, A., Catanzariti, G., Jimeno, A., Campuzano, S. A., Benito-Batanero, J. P., et al. (2016). New archaeomagnetic data recovered from the study of celtiberic remains from central Spain (Numantia and Ciadueña, 3rd-1st centuries BC). Implications on the fidelity of the Iberian paleointensity database. *Physics of the Earth and Planetary Interiors*, *260*, 74–86. https://doi.org/10.1016/j.pepi.2016.09.006

Osete, M. L., Molina-Cardín, A., Campuzano, S. A., Aguilella-Arzo, G., Barrachina-Ibáñez, A., Falomir-Granell, F., et al. (2020). Two archaeomagnetic intensity máxima and rapid directional variation rates during the Early Iron Age observed at the Iberian coordinates. Implications on the evolution of the Levantine Iron Age Anomaly. *Earth and Planetary Science Letters*, *533*, 116047. https://doi.org/10.1016/j.epsl.2019.116047

Palencia-Ortas, A., Osete, M. L., Campuzano, S. A., McIntosh, G., Larrazabal, J., Sastre, J., & Rodriguez-Aranda, J. (2017). New archaeomagnetic directions from Portugal and evolution of the geomagnetic field in Iberia from Late Bronze Age to Roman Times. *Physics of the Earth and Planetary Interiors*, *270*, 183–194. https://doi.org/10.1016/j.pepi.2017.07.004

Paterson, G. A., Tauxe, L., Biggin, A. J., Shaar, R., & Jonestrask, L. C. (2014). On improving the selection of Thellier- type paleointensity data. *Geochemistry, Geophysics, Geosystems*, *15*, 1180–1192. https://doi.org/10.1002/2013GC005135

Pavón-Carrasco, F. J., Campuzano, S. A., Rivero-Montero, M., Molina-Cardín, A., Gómez-Paccard, M., & Osete, M. L. (2021). SCHA.DIF.4k: 4000 years of paleomagnetic reconstruction for Europe and its application for dating. *JGR Solid Earth*, *126*(3).

Pavón-Carrasco, F. J., Rodríguez-González, J., Osete, M. L., & Miguel, J. (2011). A Matlab tool for archaeomagnetic dating. *Journal of Archaeological Science*, *38*, 408–419. https://doi.org/10.1016/j.jas.2010.09.021

Pressling, N., Brown, M. C., Gratton, M. N., Shaw, J., & Gubbins, D. (2007). Microwave paleointensities from Holocene age Hawaiian lavas: Investigations of magnetic properties and comparison with thermal paleointensities. *Physics of the Earth and Planetary Interiors*, *162*, 99–118. https://doi.org/10.1016/j.pepi.2007.03.007

Pressling, N., Laj, C., Kissel, C., Champion, D., & Gubbins, D. (2006). Paleomagnetic intensities from 14C-dated lava flows on the Big Island, Hawaii: 0–21 kyr. *Earth and Planetary Science Letters*, *247*, 26–40. https://doi.org/10.1016/j.epsl.2006.04.026

Rivero-Montero, M., Gómez-Paccard, M., Kondopoulou, D., Tema, E., Pavón-Carrasco, F. J., Aidona, E., et al. (2021). Geomagnetic field intensity changes in the Central Mediterranean between 1500 BCE and 150 CE: Implications for the Levantine Iron Age Anomaly evolution. *Earth and Planetary Science Letters*, *557*, 116732. https://doi.org/10.1016/j.epsl.2020.116732

Roberts, A. P., Tauxe, L., Heslop, D., Zhao, X., & Jiang, Z. X. (2018). A critical appraisal of the "Day Diagram". *Journal of Geophysical Research: Solid Earth*, *123*(4), 2618–2644. https://doi.org/10.1002/2017JB015247

Shaar, R., Tauxe, L., Ben-Yosef, E., Kassianidou, V., Lorentzen, B., Feinberg, J. M., & Levy, T. E. (2015). Decadal-scale variations in geomagnetic field intensity from ancient Cypriot slag mounds. *Geochemistry, Geophysics, Geosystems*, *16*, 195–214. https://doi.org/10.1002/2014GC005455

Shaar, R., Tauxe, L., Goguitchaichvili, A., Devidze, M., & Licheli, V. (2017). Further evidence of the Levantine Iron Age geomagnetic anomaly from Georgian pottery. *Geophysical Research Letters*, *44*(5), 2229–2236. https://doi.org/10.1002/2016gl071494

Stacey, F. D. (1967). The Koenigsberger ratio and the nature of thermoremanence in igneous rocks. *Earth and Planetary Science Letters*, *2*, 67–68. https://doi.org/10.1016/0012-821x(67)90174-4

Tauxe, L., & Yamazaki, T. (2015). Paleointensities. In G. Schubert (Ed.), *Treatise on geophysics* (2nd ed., Vol. 5, pp. 461–509). Oxford: Elsevier. https://doi.org/10.1016/b978-0-444-53802-4.00107-x

Tema, E., Hedley, I., Pavón-Carrasco, F. J., Ferrara, E., Gaber, P., Pilides, D., et al. (2021). The directional occurrence of the Levantine geomagnetic field anomaly: New data from Cyprus and abrupt directional changes. *Earth and Planetary Science Letters*, *557*, 116731. https://doi.org/10.1016/j.epsl.2020.116731

Thellier, E., & Thellier, O. (1959). Sur l'intensité du champ magnétique terrestre dans le passé historique et géologique. *Annales de Geophysique*, *15*, 285–376.

Valet, J. P., Brassart, J., Le Meur, I., Soler, V., Quidelleur, X., Tric, E., & Gillot, P. Y. (1996). Absolute paleointensity and magnetomineralogical changes. *Journal of Geophysical Research*, *101*(B11), 25029–25044. https://doi.org/10.1029/96jb02115

Veitch, J., Hedley, I., & Wagner, J. J. (1984). An investigation of the intensity of the geomagnetic field during roman times using magnetically anisotropic bricks and tiles. *Archeological Sciences*, *37*, 359–373.

Wang, H., & Kent, D. V. (2021). RESET: A method to monitor thermoremanent alteration in Thellier-series paleointensity experiments. *Geophysical Research Letters*, *48*, e2020GL091617. https://doi.org/10.1029/2020GL091617

Yu, Y. J., & Tauxe, L. (2005). Testing the IZZI protocol of geomagnetic field intensity determination. *Geochemistry, Geophysics, Geosystems*, *6*. https://doi.org/10.1029/2004GC000840